Refereed Proceedings

Heat Exchanger Fouling and Cleaning: Fundamentals and Applications

Engineering Conferences International *Year* 2003

Numerical Simulation of the Fouling on Structured Heat Transfer Surfaces (Fouling)

Fahmi Brahim* Wolfgang Augustin†
Matthias Bohnet‡

*Technical University Braunschweig
†Technical University Braunschweig
‡Technical University Braunschweig

NUMERICAL SIMULATION OF THE FOULING ON STRUCTURED HEAT TRANSFER SURFACES (FOULING)

Fahmi Brahim, Wolfgang Augustin, Matthias Bohnet

Institute for Chemical and Thermal Process Engineering, Technical University Braunschweig
Langer Kamp 7, D-38106 Braunschweig, Germany
T: +49 531 3912781 F: +49 531 3912792 E-mail: ictv@tu-bs.de

ABSTRACT

The objective of this work is to make a contribution to a good and fast prediction of the crystal growth on flat and structured heat transfer surfaces. For the numerical simulation the CFD code Fluent is used. The simulation enables an unsteady calculation of the fouling process and a realistic description of the temporal modification of the flow and temperature fields due to the continuous crystal growth.

The numerical simulation of the crystal growth is based on models for the calculation of the deposition (Krause, 1993) and removal (Bohnet, 1990) mass rates. Based on experimental results of Hirsch (Bohnet et. al., 1999), a model was developed which enables the calculation of the density of the fouling layer not only as a function of the local position within the fouling layer, but also as a function of the time-dependent total thickness of the fouling layer. In addition a model was developed, that enables a realistic distribution of the heat flux along the heat transfer surface during the simulation. All models are implemented into the simulation with the help of the programming user interface of the CFD code.

During the experimental and numerical investigations the operating parameters like flow rate, surface temperature, concentration of the salt solution and geometry of the flow channel are varied. The induction period and the effects of aging which occur with almost all fouling processes are not considered.

Result of the numerical simulation is the prediction of the fouling resistance as function of time. In view of the complexity of the fouling process during the incrustation of heat transfer surfaces and the fact that not all influences from the used models could be considered the agreement between calculated and experimentally obtained data is satisfactory.

INTRODUCTION

An analytical description resulting from complex combinations of different fouling mechanisms is not yet possible. Models have been developed at the University of Braunschweig for single fouling mechanisms such as crystallization or sedimentation. These models have been added to a CFD code for the numerical simulation of heat and mass transfer. The results enable a fast and cost favourable prediction of the fouling behaviour.

In a preliminary calculation the simple case of parallel flow past flat plates is investigated. Using this simplification numerous fouling experiments under different conditions were performed. The measurements were taken using aqueous solutions of $CaSO_4$ and serve for the verification of the numerical simulation.

EXPERIMENTAL SET-UP

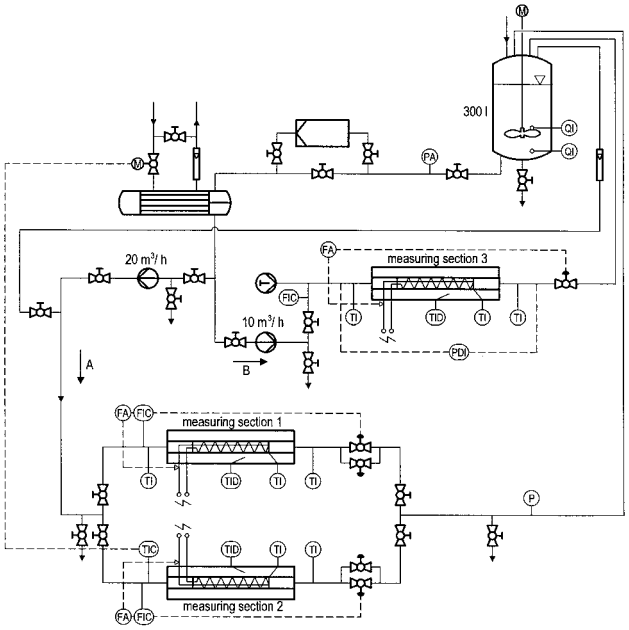

Fig. 1: experimental Set-up

Fig. 1 is a schematic diagram of the experimental unit used for fouling experiments. The centerpiece of the experimental set-up consists of three measuring sections. The second and third test sections are annular test tubes. The first test section includes a plate heat exchanger suited for a comfortable replacement of its heat transfer surface. The salt concentration of the aqueous calcium sulphate solution is controlled by conductimetry. Two centrifugal pumps provide a continuous flow of liquid through the system. The solution is passed from a storage tank through a heat exchanger which controls the inlet temperature and then to the measuring sections. The filter avoids sedimentation of particles and secondary nucleation in the test sections, since seed particles can influence nucleation behaviour considerably. The heat exchanger guarantees a

constant inlet temperature at the test sections. The liquid flow is divided and flows to the two measuring sections, each equipped with a flowmeter and a flow controller. After passing through the two measuring sections the two partial streams are recombined and fed back to the storage tank. Due to a relatively large volume of liquid in the storage tank, the decline of the concentration of salt in the solution throughout the fouling period is rather slow. Regular addition of calcium sulfate hemihydrate to the storage tank maintains a relatively constant concentration. The heat exchanger surfaces of the measuring sections are heated electrically allowing for operation at constant heat flux.

GEOMETRICAL FLOW MODEL

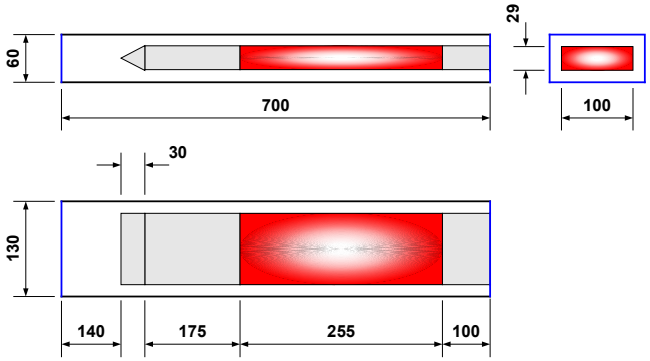

Fig. 2: Geometrical flow model (measuring section 1)

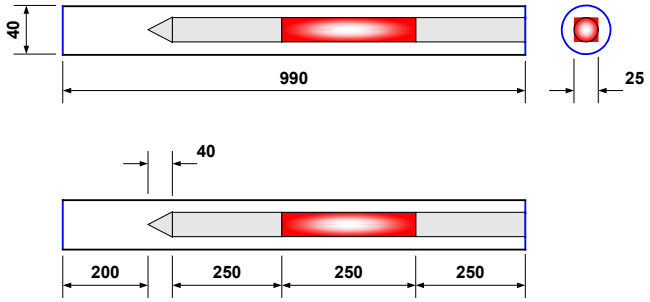

Fig. 3: Geometrical flow model (measuring section 2)

The dimensions of the geometrical flow models used by the numerical simulation are represented in Fig. 2 and Fig. 3 Deviations between 2D and 3D simulation calculations regarding flow rate and surface temperature distribution were minimal. Since the computational effort and cost in terms of CPU time and memory of the 3D simulation is very high, the flow case was regarded as two dimensional.

The discretization of the computing area was performed with an unstructured grid. The dissolution of the grid is usually adapted to the flow velocity and temperature gradients, so that a finer discretization takes place in radial direction to the channel wall and in axial direction particularly in the area above the heat transfer surface and its pre- and wake ranges. The wall near cells of the computation lattice contain the laminar viscous sublayer and the transient area. In these cells the two-zonal-model for the computation of the flow velocity and temperature gradients, described in the next section, is used.

TURBULENCE MODEL AND MODELING OF THE WALL REGION

The simplest "complete models" of turbulence are two-equation models in which the solution from two separate transport equations allows the turbulent velocity and length scales to be determined independently. The standard k-ε model falls within this class of turbulence models. It is a semi-empirical model and the derivation of the model equations relies on phenomenological considerations and empiricism. By the numerical simulation the realizable k-ε model was used. It offers the following advantages compared to the standard model (Fluent, 2003):

1. The possibility of usage not only with high Reynolds-number flows (Re $>$ 50000) but also with small Reynolds-number and transient flows (2300 $<$ Re $<$ 10000).
2. The realizable k-ε model satisfies certain mathematical constraints on the Reynolds stresses, consistent with the physics of turbulent flows.

The turbulence models are primarily valid for turbulent core flows (i.e. the flow in the regions somewhat far from walls). Therefore consideration needs to be given to an adaption for wall-bounded flows.

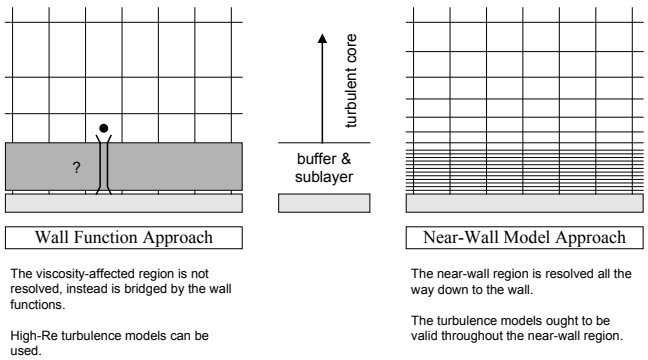

Fig. 4: Near-wall treatments in Fluent

There are two approaches for modeling the near-wall region. In one approach the viscosity affected inner region (viscous sublayer and buffer layer) is not resolved. Instead, semi-empirical formulas called wall functions are used to bridge the viscosity affected region between the wall and the fully-turbulent region. In the second model, named the "two-layer zonal model", the wall functions are completely abandoned in favour of resolving the viscosity affected near-wall region all the way to the viscous sublayer. In the

two-layer model, the entire domain is subdivided into a viscosity affected region and a fully turbulent region (Fig. 4).

The wall function approach, however, is inadequate in situations where the low-Reynolds number (Re < 10000) effects are pervasive throughout the flow domain in question, and therefore the hypotheses underlying the wall functions cease to be valid. Such situations require near-wall models that are valid in the viscosity affected region and accordingly integrable all the way to the wall.

NUMERICAL SIMULATION OF THE CRYSTAL GROWTH

The CFD program Fluent can be used for the simulation of flows with heat and mass transfer procedures. It enables the computation of the flow and temperature field. The simulation of the fouling process and crystal growth on heat transfer surfaces with the original version of Fluent is however not possible. The CFD code offers therefore the possibility to add own models in a form of user defined subroutines.

The following models, which are necessary for the simulation of the fouling process, were implemented in Fluent with user defined subroutines (UDS):

- Computation of the deposition mass rate
  - Saturation concentration
  - diffusion coefficient
  - mass transfer coefficient
- computation of the density of the fouling layer
- computation of the removal mass rate
- computation of the heat transfer
  - distribution of the heat flow density along the heat transfer surface
  - heat conductivity of the fouling layer
- computation of the total rate, layer thickness and fouling resistance

Deposition mass rate

By numerical calculation of the deposition mass rate $\dot{m}_d$ the mass transfer resistance between bulk and interface salt solution/crystal layer was considered. Thus the concentration profile in the bulk and in the laminar boundary layer can be presented as shown in Fig. 5.

The deposition process of calcium sulfate on heat transfer surfaces can be divided into two subprocesses. In a first step the calcium and sulfate ions are transported by diffusion and convection from the bulk to the phase boundary salt solution/crystal layer. In a second step the transported ions are built into the crystal lattice. Investigations of A.R. Konak (1974) showed that the order of the surface reaction corresponds to the number of ions that take part in the crystallization reaction. The order of a crystallization reaction from a solution, in which Ca^{++} - and SO_4^{--} are present, is therefore n = 2. This reaction order was confirmed by a set of investigations of different authors. S.T. Liu and G.H. Nancollas (1970) for $CaSO_4$ and P. Courvoisier et al. (1970) for $CaSO_4 1/2\ H_2O$ determined a reaction order of n = 2.

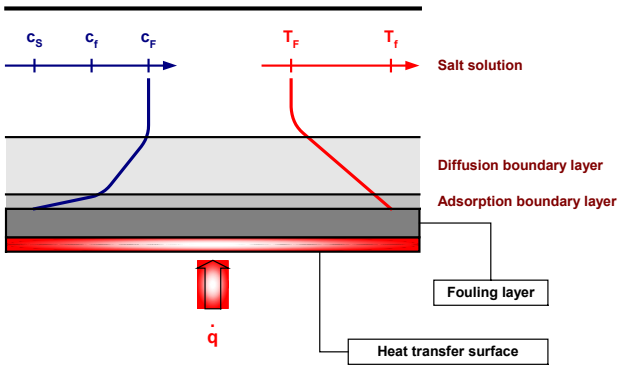

Fig. 5: Concentration and temperature profile in the vicinity of the fouling layer (fouling by crystallization)

If it is assumed that all ions transported to the phase boundary participate in the surface reaction, the equations for the calculation of the transported and inserted mass rates can then be combined by eliminating the unknown concentration c_f at the phase boundary. The combination leads to a relationship for the calculation of the deposition mass rate that considers the mass transfer resistance (Brahim, 2001):

$$\dot{m}_d = \beta \cdot \left[\frac{1}{2}\frac{\beta}{k_R} + \Delta c - \left(\frac{1}{4}\left(\frac{\beta}{k_R}\right)^2 + \frac{\beta}{k_R}\cdot\Delta c \right)^{1/2} \right] \qquad (1)$$

c_S is the saturation concentration and is calculated as a function of T_f at the phase boundary (Lammers, 1972):

$$\log(c_S) = -\frac{a_1}{2.3\cdot\Re\cdot T_f} + \frac{a_2}{\Re}\cdot\log(T_f) + a_3 \qquad (2)$$

Table 1. Model coefficients for the calculation of the saturation concentration (Eq. 2)

	$CaSO_4\ 2H_2O$	$CaSO_4\ ½\ H_2O$	$CaSO_4$
a_1	-33731.93	-35378.23	-44550.53
a_2	-108.87	-162.38	-183.04
a_3	37.75	54.56	61.83

For the determination of the diffusion coefficient of calcium sulfate in aqueous solution a computing model based on calculation results of Lammers (1972) was developed. This model describes the dependency of the diffusion coefficient on the two parameters temperature and concentration:

$$D(T,c)=\frac{b_1\cdot T^3+b_2\cdot T^2+b_3\cdot T+b_4}{c+1}+b_5\cdot T^3+b_6\cdot T^2+b_7\cdot T+b_8 \quad (3)$$

Table 1. Model coefficients for the calculation of the diffusion coefficient (Eq. 3)

b_1	b_2	b_3	b_4
3.923e-16	2.333e-15	7.153e-12	1.049e-10
b_5	b_6	b_7	b_8
-2.539e-16	1.087e-13	1.036e-11	2.769e-10

The mass transfer coefficient can be determined as a function of the Sherwood number and the diffusion coefficient:

$$\beta=\frac{Sh\cdot D}{d_h} \quad (4)$$

For the calculation of the Sherwood number a semiempirical approach according to Lammers (1972) was used:

$$Sh=0.034\cdot Re^{0.875}\cdot Sc^{1/3} \quad (5)$$

Density of the fouling layer

The density of the fouling layer is one of the most important quantities for the calculation of the fouling resistance. It does not only affect the calculation of the removal mass rate but also the calculation of the layer thickness itself. A cross section of a fouling layer shows that the layer is not homogeneous. In most case 4 layers can be differentiated, which are different in the structure, color and strength.

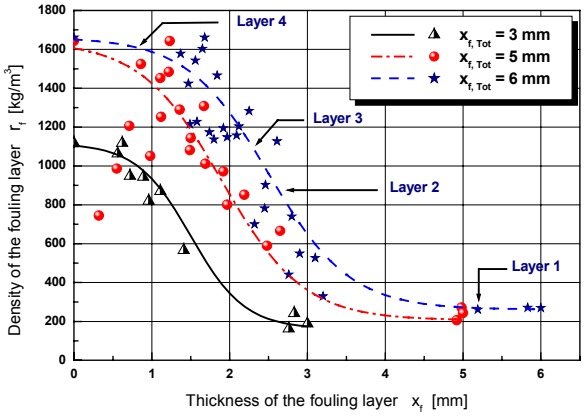

Fig. 6: Local density ρ_f versus total thickness of the fouling layer (Hirsch, 1996)

Hirsch (1996) noticed that the density of the fouling layer depends not only on the local position in the layer but also on the total thickness of the crystal layer. For the numerical simulation it is necessary to calculate both unsteady and local values of the density of the fouling layer because of the relationship between time and the calculated total thickness of the crystal layer (Fig. 6).

Based on results of abrasion experiments and by neglecting the aging effect of the crystal layer the following computer model was developed and integrated into the numerical simulation. It describes a unique relationship between the density of the fouling layer ρ_f and the two parameters; local position within the fouling layer x_f and total thickness of the fouling layer $x_{f,Tot}$.

$$\rho_f(x_f,x_{f,Tot})=c_2+\frac{c_1-c_2}{1+10^{\left(\frac{x_f-c_3}{c_4}\right)}} \quad (6)$$

Table 3: Model coefficients for the calculation of the density of the fouling layer

c_1	$10^3\cdot\log\left(1.11+0.7\cdot x_{f,Tot}\right)$
c_2	$105+22.5\cdot x_{f,Tot}$
c_3	$0.5\cdot x_{f,Tot}$
c_4	$0.25\cdot x_{f,Tot}$

Removal mass rate

For the calculation of the removal mass rate the following approach was used (Bohnet 1987):

$$\dot{m}_r=\frac{K}{P}\cdot\rho_f\cdot(1+\delta\cdot\Delta T)\cdot d_p\cdot\left(\rho^2\cdot\eta\cdot g\right)^{1/3}\cdot x_f\cdot w^2 \quad (7)$$

w is the local value of the flow velocity above the crystal layer. P describes the intercrystalline adhesion forces. K is a parameter that is equal to the number of fault points in the fouling layer. $(1+\delta\cdot\Delta T)$ describes the temperature stresses in the fouling layer. δ is the linear expansion coefficient and ΔT the temperature gradient in the fouling layer. d_p is the mean crystal diameter.

Heat transfer

The thermal conductivity can be calculated, based on measurement results of the porosity of the fouling layer. It is computed by the thermal conductivity of the pore medium (λ_{Water} = 0,67 W/m K) and the compact solid (λ_{Gypsum} = 1.3 W/m K). After considerations of O. Krischer (1978) over the thermal conductivity of porous systems two limit curves for the thermal conductivity of the material system gypsum/water for parallel joined resistances is represented through:

$$\lambda_{f,I}=\varepsilon\cdot\lambda_{Water}+(1-\varepsilon)\cdot\lambda_{Gipsum} \quad (8)$$

and accordingly for in series connected resistances through:

$$1/\lambda_{f,II}=\varepsilon/\lambda_{Water}+(1-\varepsilon)/\lambda_{Gipsum} \quad (9)$$

The thermal conductivity of the fouling layer is then computed as the arithmetic average value of both limit values:

$$\lambda_f = \left(\lambda_{f,I} + \lambda_{f,II}\right)/2 \qquad (10)$$

The graphical evaluations of Eq. (8) and Eq. (9) for the entire porosity range $\varepsilon = 0 \cdots 1$ are represented in Fig. 7. The mean values according to the dash-dotted lines are approximations of the thermal conductivity of the porous fouling layer in accordance with Eq. (10). The measured porosity range, in Fig. 7 represented as a hatched area, lies between 5 and 15 %. On the average a mean porosity of $\bar{\varepsilon} = 10$ % was measured. It follows:

$$\lambda_f = 1.2\ \mathrm{W/m \cdot K} \qquad (11)$$

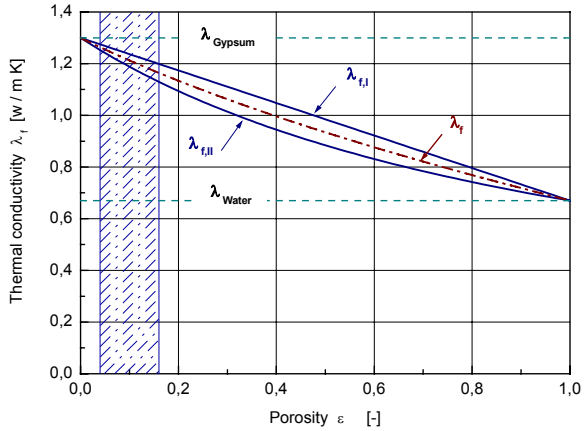

Fig. 7: Thermal conductivity λ_f versus porosity of the fouling layer

The definition of a constant and from the local position along the heat transfer surface independent distribution of the heat flux in the numerical simulation is not permissible. This leads to the computation of temperature distributions along the heat transfer surface and/or phase boundary crystal layer/salt solution, which rises continuously in flow direction. This leads again to a not realistic calculation of the fouling layer thickness distribution. The numerical simulation supplies an unrealistic profile of the fouling layer.

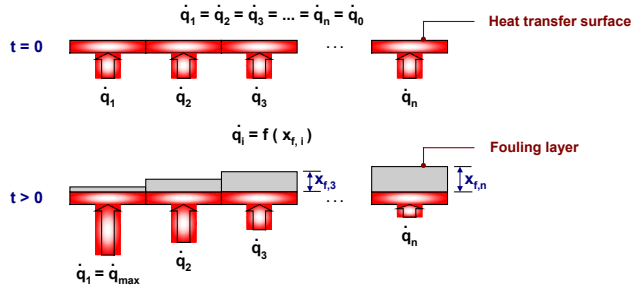

Fig. 8: Principle of the realistic distribution of the heat flux along the heat transfer surface

In reality the heat flows through the section of the fouling layer with the smallest thermal resistance. Therefore a local and unsteady heat flux distribution along the heat transfer surface is formed (Fig. 8).

The maximal heat flux $\dot{q}_{max}$ will flow through the wall cell with the thinnest crystal layer. Through each other cell flows a heat flux $\dot{q}_i$, which can be calculated as follows:

$$\dot{q}_i = \frac{x_{f,min}}{x_{f,i}} \cdot \frac{\sum_{i=1}^{n} \frac{x_{f,min}}{x_{f,i}}}{n \cdot \dot{q}_0} \qquad (12)$$

Equation (12) states that the larger the layer thickness $x_{f,i}$ above the wall cell i the smaller the heat flux $\dot{q}_i$ that flows through it. Visual Observation of the fouling layer shows a local distribution of the thickness along the heat transfer surface.

Total rate, layer thickness and Fouling resistance

The total mass transfer rate $\dot{m}$ is calculated as the difference between the deposited and removed mass rates. The results of the numerical simulation are shown in Fig. 9. The decrease of the deposition mass rate per unit time can be explained by considering the decrease in surface temperature of the fouling layer. This occurs because of higher fluid velocities and therefore an improved heat transfer. The increase of the mass transfer coefficient due to the flow rate acceleration is very small and does not considerably affects the calculation of the deposition mass rate.

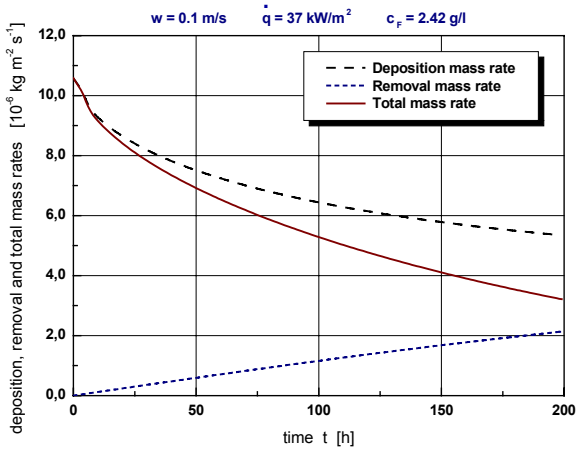

Fig. 9: Temporal progression of deposition, removal and total mass rates

The removed mass rate increases with time. This increase can be explained after considering the increase in flow rate and the growth of the crystal layer, on the heating element. The increase in flow rate contributes to the rise of

the wall shear stress, while the growth of the crystal layer increases the temperature stress within the fouling layer.

The calculation of the average total thickness of the fouling layer until the time $t + \Delta t$ is calculated as the sum of the average total thickness from time t and the new growth within the time step Δt :

$$x_{f,t+\Delta t} = x_{f,t} + \frac{\dot{m} \cdot \Delta t}{\rho_f} \qquad (13)$$

With the determined total thickness and assuming constant thermal conductivity the fouling resistance can then be calculated as:

$$R_{f,t+\Delta t} = \frac{x_{f,t+\Delta t}}{\lambda_f} \qquad (14)$$

RESULTS

Comparison measurement/simulation (flat heat transfer surfaces)

Fouling experiments with different calcium sulfate concentrations ($c_F = 2.22 \cdots 2.89\ g/l$) flow rates ($w = 0.05 \cdots 0.37\ m/s$) and heat fluxes ($\dot{q} = 31 \cdots 97\ kW/m^2$) were carried out.

Fig. 10 to 12 show the measured and numerically calculated values of the fouling resistance versus time for different values of the flow velocity, heat flux and concentration of the salt solution.

The agreement between measurement and simulation is satisfactory. The form of the fouling curves can be reproduced by the simulation. Generally, the calculated values of the fouling resistance are smaller then the measured values.

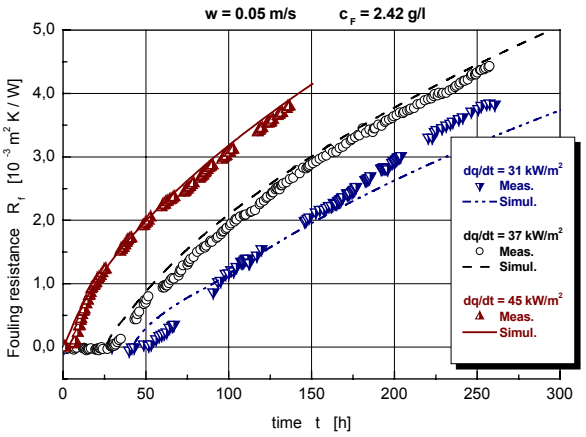

Fig. 10: Measured and simulated values of the fouling resistance versus time for different heat fluxes (measuring section 1)

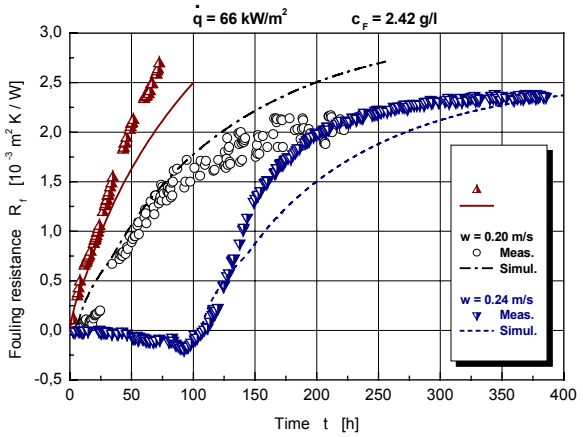

Fig. 11: Measured and simulated values of the fouling resistance versus time for different flow rates (measuring section 2)

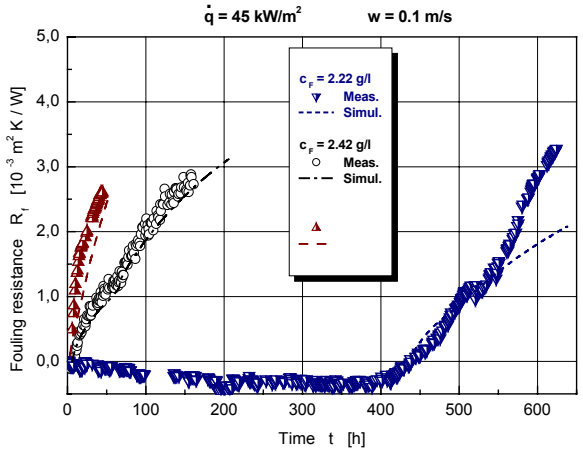

Fig. 12: Measured and simulated values of the fouling resistance versus time for different concentrations of the salt solution (measuring section 1)

A considerable deviation (50 %) between measurement and simulation accured for the case of a low concentration of CaSO4. In this case the gradient of the measured fouling curve increases after a long induction period and remained then constant until the end of the experiment. The gradient of the simulated Fouling curve decreases however continuously.

Comparison measurement/simulation (structured heat transfer surfaces)

Table 4. Height of the ribs of the structured heat transfer surfaces (forms 1 to 6)

	Meas. + Simul.			Only Simul.			
Form	0	1	2	3	4	5	6
Height [mm]	0	8	8	8	4	2	1

Two experiments with structured geometries (Form 1 and 2) were accomplished. Further geometries were only simulated (Form 3 to 6). The operating parameters are held constant for all forms ($w = 0.05\ m/s$, $\dot{q} = 45\ kW/m^2$ and $c_F = 2.42\ g/l$). Form 0 means an unstructured (flat) heat transfer surface. Difference between the forms 3 to 6 lies only in the height of the structure (Tab. 4). All assigned forms of the heat transfer surface are represented schematically in Fig. 13.

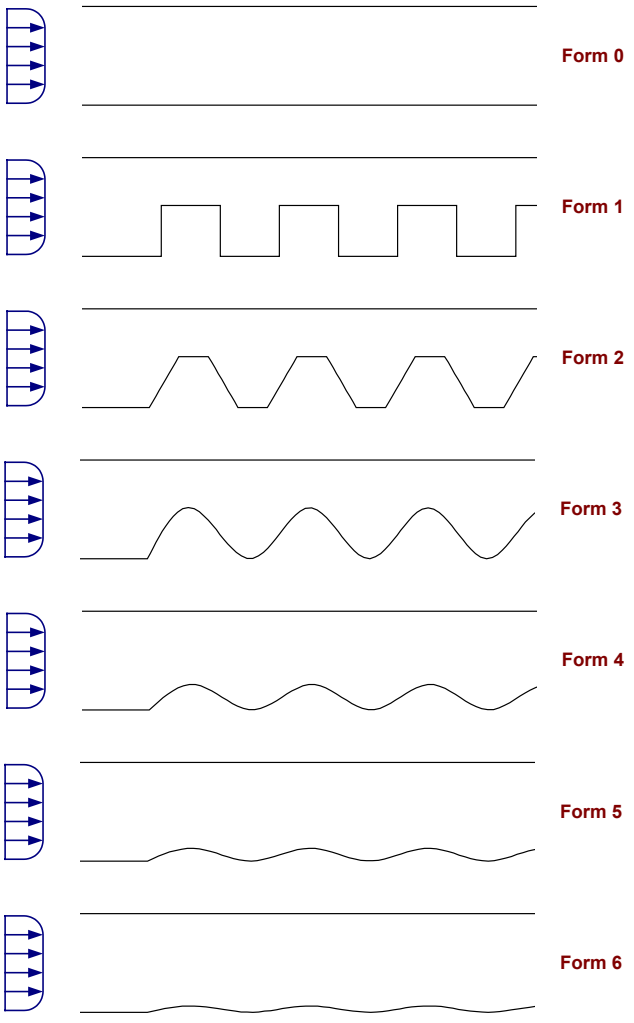

Fig. 13: Different forms of the structured heat transfer surfaces

Fig. 14 shows a comparison between measurement and simulation by the forms 0, 1 and 2 of the heat transfer surface. The results confirm the improvement of the fouling behaviour by structured geometries noticed by Augustin (1993).

The influence of the height of the structures by the same form and the same number of ribs is seen in Fig. 15. The wavy form is thereby selected and the height of the ribs is changed between 8 and 1 mm. As comparison curve the calculated values of the fouling resistance versus time by the form 0 is also represented.

Based on all simulation results with structured geometries of the heat transfer surface, we can state that the form 3, due to the successful combination between high turbulence and good flow guidance (Fig. 16), exhibits the most favourable fouling behaviour.

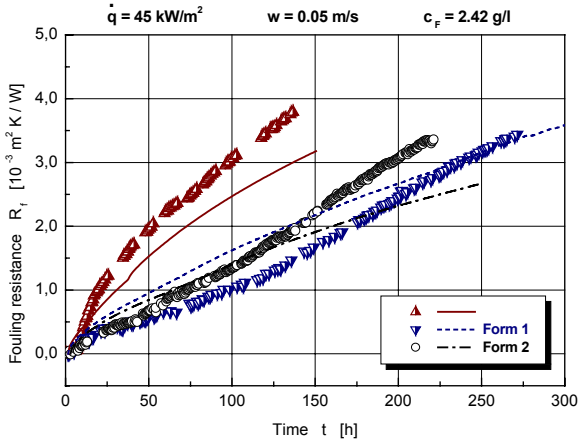

Fig. 14: Comparison Measurement/Simulation for unstructured (form 0) and structured (form 1 and 2) heat transfer surfaces

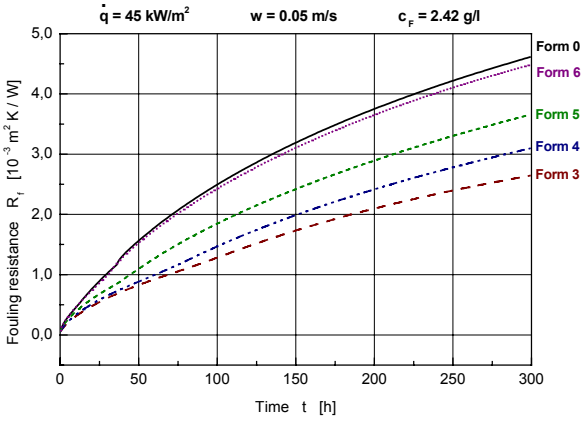

Fig. 15: Simulated values of the fouling resistance versus time for unstructured (form 0) and structured (form 3 to 6) heat transfer surfaces.

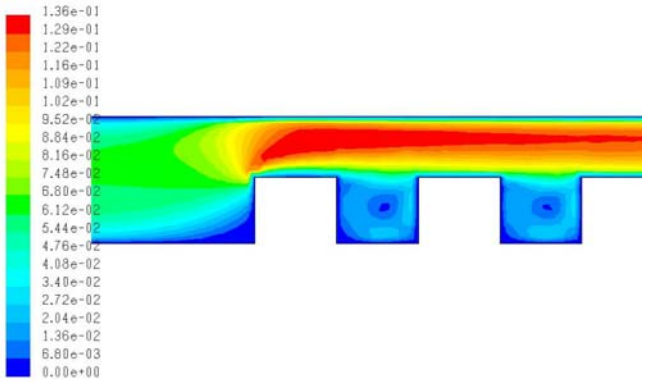

Form 1

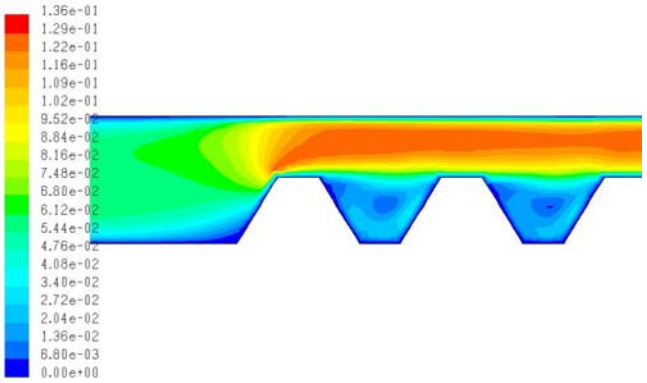

Form 2

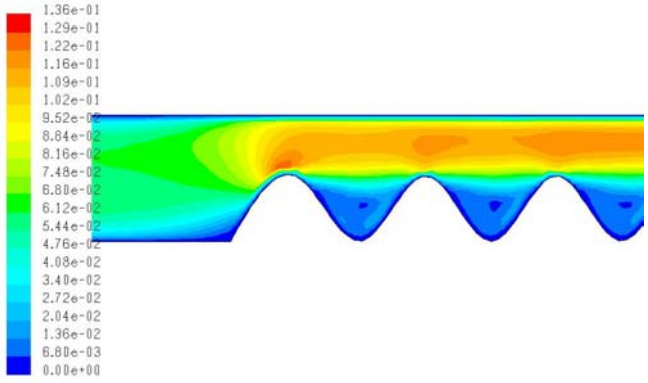

Form 3

Fig. 16: contour plots of the flow velocity above the heat transfer surface for the forms 1, 2 and 3

CONCLUSIONS AND PROSPECT

Objective of this work is to provide a simple, fast and cost favourable computation method which enables a good prediction of the fouling behaviour. The used CFD code for the numerical simulation enables the computation of the flow and temperature fields. For the simulation of the crystal growth it was necessary to add own models to the CFD code via user defined subroutines.

The agreement between measurement and simulation is generally satisfactory. The simulation however tends in most cases to underestimate the fouling behaviour. Reason for that is the fact that Fluent computes too small values of the temperature at the phase boundary crystal layer/salt solution. Particularly for the examined flow rate range ($w = 0.05 \cdots 0.35\ m/s$) the deviation between measurement and simulation, regarding temperature at the phase boundary, can not be neglected.

The numerical simulation of the crystal growth on heat transfer surfaces exhibits a large research potential. Not only optimisation steps by the computation of the temperature at the phase boundary crystal layer/salt solution are necessary, but also the roughness of the fouling layer, the induction period and the consideration of the aging process must be modelled and implemented into the simulation. Future research has as target also the improvement of the computer models used and the 3D simulation of the fouling process

KNOWLEDGEMENT

The financial support for this research work has been granted by “Deutsche Forschungsgemeinschaft (DFG)”.

FORMULA DIRECTORY

$a_1 \cdots a_3$	Constant	[-]
$b_1 \cdots b_8$	constant	[-]
$c_1 \cdots c_4$	constant	[-]
$c,\ c_F$	concentration of salt solution	[kg/m^3]
c_S	saturation concentration	[kg/m^3]
c_f	concentration in the vicinity of the fouling layer	[kg/m^3]
D	diffusion coefficient	[m^2/s]
d_h	hydraulic diameter	[m]
d_p	mean crystal diameter	[m]
g	gravitational acceleration	[m/s^2]
P/K	cohesion coefficient	[kg m/s^2]
k_R	rate of reaction	[m^4 kg/s]
$\dot{m}$	total mass rate	[kg/m^2 s]
$\dot{m}_d$	deposition mass rate	[kg/m^2 s]
$\dot{m}_r$	removal mass rate	[kg/m^2 s]
n	order of the surface reaction	[-]
n	number of wall cells along the heat transfer surface	[-]
P	intercrystalline adhesion force	[N]

$\dot{q}$	heat flux	[W/m^2 K]
R_f	fouling resistance	[W/m^2 K]
$\Re$	Universal gas constant	[J/mol.k]
T_f	temperature of fouling layer surface	[K]
T_F	temperature of salt solution	[K]
x_f	thickness of crystal layer	[m]
$x_{f,\,min}$	Thickness of the thinnest crystal layer along the heat transfer surface	[m]
w	fluid velocity	[m/s]
δ	linear expansion coefficient	[K^{-1}]
Δt	Computing time step	[*s*]
ΔT	temperature gradient	[K]
Δc	Concentration gradient = c_F - c_S	[kg/m^3]
ρ	density of salt solution	[kg/m^3]
ρ_f	density of fouling layer	[kg/m^3]
λ_f	thermal conductivity of the fouling layer	[W/m K]
β	mass transfer coefficient	[m/s]
η	viscosity of salt solution	[kg/m s]
Re	Reynolds number	[-]
Sh	Sherwood number	[-]
Sc	Schmidt number	[-]
ε	Porosity	[-]

REFERENCES

S. Krause, *Fouling of heat transfer surfaces by crystallization and sedimentation*, Int. Chem. Eng. 33 (1993) 3, S. 355-401

M. Bohnet, *Fouling of heat transfer surfaces*, Chem. Eng. Techn. 10 (1987) 2, S. 113/125

M. Bohnet, W. Augustin, H. Hirsch, *Influence of fouling layer shear strength on removal behaviour, Proceedings of an international conference of understanding heat exchanger fouling and its mitigation*, Castelvecchio Pascoli, Italy,Hrsg. T.R Bott, Begell House, Inc. New York, 1999, S. 201-208

Fluent Inc., FLUENT User's Guide Release 6.0 (2003)

A. R. Konak, *A new model for surface reaction-controlled growth of crystals from solution*, Kali Chem. Engng. Sci. Bd. 29 (1974) Nr. 7. S. 1537/43

S. T. Liu, G.H. Nancollas, *The Kinetics of crystal growth of calcium sulfate dihydrate*, Kali J. Crystal Growth (1970), Nr. 6, 281/89

P. Courvoisier, *Étude de la formation des Dépôts de Sulfate de calcium sur paroi fixe,* , Kali 3rd. Int. Symp. on fresh water from cea (1970) Nr. 1, S. 439/54

F. Brahim , W. Augustin, M. Bohnet, *Numerical Simulation of Crystal Growth on Heat Transfer Surfaces,* Proceedings of the Heat Exchanger Fouling Fundamental Approaches \& Technical Solutions, 08.-13.07.2001, Davos, Switzerland, United Engineering Foundation, New York

J. Lammers, *Zur Kristallisation von Calciumsulfat bei der Verkrustung von Heizflächen*, Diss. TU Berlin (1972)

O. Krischer, *Die wissenschaftlichen Grundlagen der Trocknungstechnik* Springer-Verlag 1978, Berlin, Heidelberg, New York

M. Bohnet., W. Augustin, *Effect of Surface Structure and pH-Value on Fouling Behaviour of Heat Exchangers*, Proceedings of 6th international Symposium on Transport Phenomena in Thermal Engineering, Seoul, Korea, 1993, S. 295-300